
XS-VID: An Extremely Small Video Object Detection Dataset

Jiahao Guo, Ziyang Xu, Lianjun Wu, Fei Gao, Wenyu Liu, Xinggong Wang
Huazhong University of Science and Technology
{gj_hust, xuzyoung, lianjunwu, gaofei_hust, liuwu, xgwang}@hust.edu.cn

Abstract

Small Video Object Detection (SVOD) is a crucial subfield in modern computer vision, essential for early object discovery and detection. However, existing SVOD datasets are scarce and suffer from issues such as insufficiently small objects, limited object categories, and lack of scene diversity, leading to unitary application scenarios for corresponding methods. To address this gap, we develop the XS-VID dataset, which comprises aerial data from various periods and scenes, and annotates eight major object categories. To further evaluate existing methods for detecting extremely small objects, XS-VID extensively collects three types of objects with smaller pixel areas: extremely small (*es*, $0 \sim 12^2$), relatively small (*rs*, $12^2 \sim 20^2$), and generally small (*gs*, $20^2 \sim 32^2$). XS-VID offers unprecedented breadth and depth in covering and quantifying minuscule objects, significantly enriching the scene and object diversity in the dataset. Extensive validations on XS-VID and the publicly available VisDrone2019VID dataset show that existing methods struggle with small object detection and significantly underperform compared to general object detectors. Leveraging the strengths of previous methods and addressing their weaknesses, we propose YOLOFT, which enhances local feature associations and integrates temporal motion features, significantly improving the accuracy and stability of SVOD. Our datasets and benchmarks are available at https://gj_hust.github.io/XS-VID/.

1 Introduction

Small Video Object Detection (SVOD) is a significant branch of computer vision and a hot topic in both academia and industry. Especially in fields such as public safety and aerial surveillance, the early discovery and detection of objects are particularly crucial. However, despite significant advancements in video object detection (VOD) techniques in recent years, small object detection in videos remains underexplored. This oversight is largely due to the lack of video datasets specifically designed for small object detection, hindering both training and evaluation processes, and consequently leading to a scarcity of effective methods.

Existing video object detection datasets suffer from insufficiently small object sizes, limited categories of objects, and insufficiently diverse scenes. As shown in Fig. 2, the pixel areas of objects in ImageNetVID, VisDrone2019VID, and UAVTD are concentrated at 187^2 , 45^2 , and 30^2 , respectively. In ImageNetVID, objects smaller than 12^2 constitute only 0.05%, while in VisDrone2019VID and UAVTD, they constitute less than 3.6%. Furthermore, UAVTD is mainly for vehicle detection with a single object category, which cannot meet the needs of multi-category small object detection, and the scenes only include traffic roads, making the scene single and not conducive to the generalization of methods. Therefore, it is urgent to develop a dataset with numerous small objects, diverse scenes, and multiple object categories for SVOD advancement.

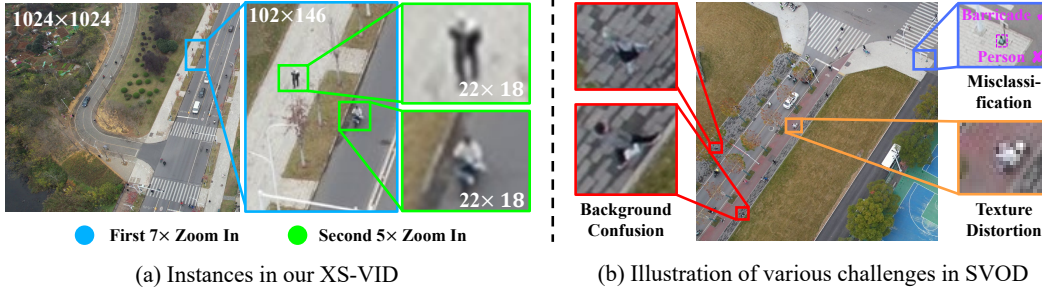


Figure 1: **Showcases of our XS-VID dataset’s object size and challenges in SVOD.** (a) shows that the objects in our XS-VID dataset are extremely small, and (b) indicates that SVOD mainly faces three challenges: background confusion, misclassification, and texture distortion.

To address these issues, we propose a video object detection dataset, XS-VID. XS-VID includes 12K frames and 38 medium-to-long sequence videos, covering multiple object sizes across 10 types of scenes, including rivers, forests, skyscrapers, and roads, at various times of day and night. The small objects in XS-VID are not concentrated at a fixed size but comprehensively cover small object sizes ranging from $0 \sim 32^2$. Specifically, the number of objects within the ranges of *es* ($0 \sim 12^2$), *rs* ($12^2 \sim 20^2$), *gs* ($20^2 \sim 32^2$), and *normal* ($>32^2$) are 49k, 94k, 36k, and 72k, respectively, accounting for 19.3%, 36.6%, 14.0%, and 30.1%. To our best knowledge, XS-VID offers the most comprehensive coverage of small object sizes, the largest number and proportion of *es* objects, and the widest range of scene types, effectively filling the existing data gap.

In addition to proposing the dataset, we further outline the existing challenges in our datasets. As shown in Fig. 1 (b), SVOD faces challenges such as: (1) Background confusion: The background texture is weak and similar in color to the object, making the object difficult to discover. (2) Easy to misclassify: Small objects have insufficient texture and contour features, easily misleading the network to make wrong classifications. (3) Texture distortion: The pixel range of small objects is extremely small, causing severe degradation of texture features. Moreover, due to the lack of datasets and benchmarks for extremely small objects, research on methods for detecting extremely small objects across various scenes and categories is also very limited. Adopting single-frame Small Object Detection (SOD) methods or Video Object Detection (VOD) methods directly does not perform well. SOD methods rely on static single-frame features for detection and lack the utilization of temporal features, failing to adequately address the three existing issues. VOD methods only focus on medium and large object sizes and the network pipeline is not suitable for extremely small objects, resulting in poor detection performance and failure to cope with the challenges of SVOD.

To address the above issues, we propose an SVOD network that integrates YOLOv8 with the recurrent all-pairs Field Transforms [25] based optical flow, named YOLOFT. Extensive experiments on XS-VID and VisDrone2019VID demonstrate that YOLOFT achieves state-of-the-art performance.

In summary, our main contributions include:

- (1) We propose the XS-VID dataset, which currently provides the most comprehensive coverage of small object sizes, the largest number and proportion of extremely small objects, and the widest range of scene types known, effectively filling the data gap;
- (2) We conduct extensive experiments to reveal the performance of various advanced detection methods on the proposed XS-VID dataset and observe that these methods often perform poorly due to lack of consideration for extremely small objects in existing datasets;
- (3) We propose a small video object detection method, YOLOFT, which significantly improves the accuracy and stability of small object detection by enhancing local feature associations and integrating temporal motion features of objects and can serve as a baseline reference for future research on XS-VID.

2 Related Work

SVOD Dataset. Small-object video detection aims to localize and classify tiny objects within continuous video frames, particularly in scenes abundant with small objects. Historically, the most

well-known video detection dataset is ImageNetVID [21], which has only 3% small objects (less than 32^2 pixels), with the majority of object sizes around 300^2 pixels, limiting its efficacy in assessing small object detection. In recent years, the VisDrone2019VID [39] dataset, collected by low-altitude drones, also features insufficiently small objects, primarily around 45^2 pixels, across over a dozen categories. NPS-Drone [15] focuses on drone detection with extremely small object sizes (about 14^2 pixels), but has a limited number of objects, averaging only one object per frame and just one category. UAVTD [34] objects vehicle detection with object sizes centered around 30^2 pixels, focusing on distinct texture features of vehicles at small scales, thus failing to comprehensively evaluate various small objects.

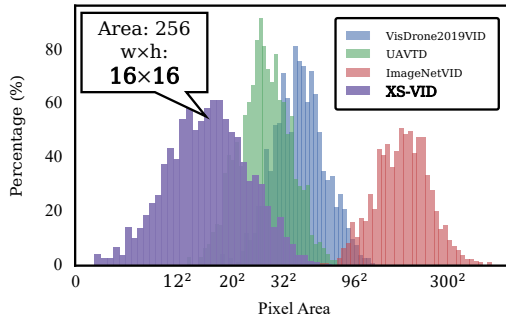


Figure 2: **Comparison of object size distribution between XS-VID and other datasets.** Our XS-VID generally has smaller object sizes.

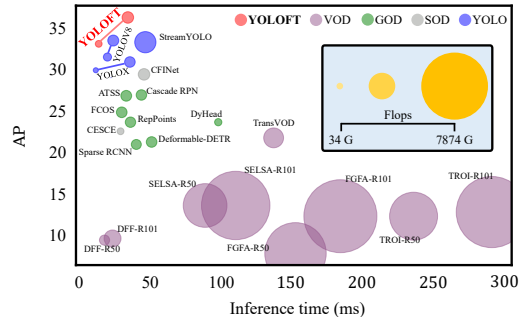


Figure 3: **AP-Latency comparison of various methods on our XS-VID.** Our YOLOFT achieves the SOTA performance.

Video Object Detection. FGFA [41] enhances inter-frame feature consistency through optical flow-guided feature aggregation. MEGA [4] utilizes a long-term memory module to enhance global and local information from past frames. SELSA [31] treats videos as unordered collections of frames and aggregates features on a sequence level via attention-based global proposal feature fusion. TROI [10] introduces a novel temporal ROI alignment operator for extracting temporal information of object instances throughout the video. DiffusionVID [20] employs a diffusion model to refine object boxes in video sequences, thereby improving denoising effects. TransVOD [38] leverages DETR’s query design to avoid complex post-processing techniques such as Seq-NMS or Tubelet rescoring. YOLOV [23] focuses on selecting key areas post-detection to reduce computational load and enhance efficiency. StreamYOLO [33] improves the accuracy and robustness of real-time video object detection through a dual-stream perception module and trend-aware loss. However, these methods often favor medium and large-sized objects or objects only a single category. This bias restricts the detectors’ generalization capabilities and minimally addresses issues like background confusion, misclassification, and texture distortion inherent in SVOD.

Small Object Detection. Due to the scarcity of small objects in previous datasets, many methods [14, 2, 35, ?] employ data augmentation to enhance detector performance for small objects. Certain approaches leverage multiscale information to explore the contextual features of small objects. Techniques based on GANs enhance the semantic representation of tiny objects by restoring their detailed features [1, 18, 13, 32]. MDvsFA [29] employs adversarial learning for detection and localization of faint infrared small objects. ScaleKD [43] enhances the model’s detection capability for small objects through cross-scale knowledge distillation. UFPMP-Det [11] combines multiscale feature fusion and a unified feature pyramid multipath design, followed by CEASC [8] which achieves faster and more accurate small object detection through adaptive sparse convolution and global context enhancement. CFNet [36] improves the precision of small object detection through coarse-to-fine candidate box generation and imitation learning. TransVisDrone [22] uses a spatiotemporal Transformer to enhance the detection accuracy of extremely small drone objects in videos. However, SOD methods rely on static single-frame features for detection, lacking the utilization of temporal features, leading to poor detection performance in the absence of distinctive texture features, and limited improvement in background confusion, misclassification, and texture distortion issues.

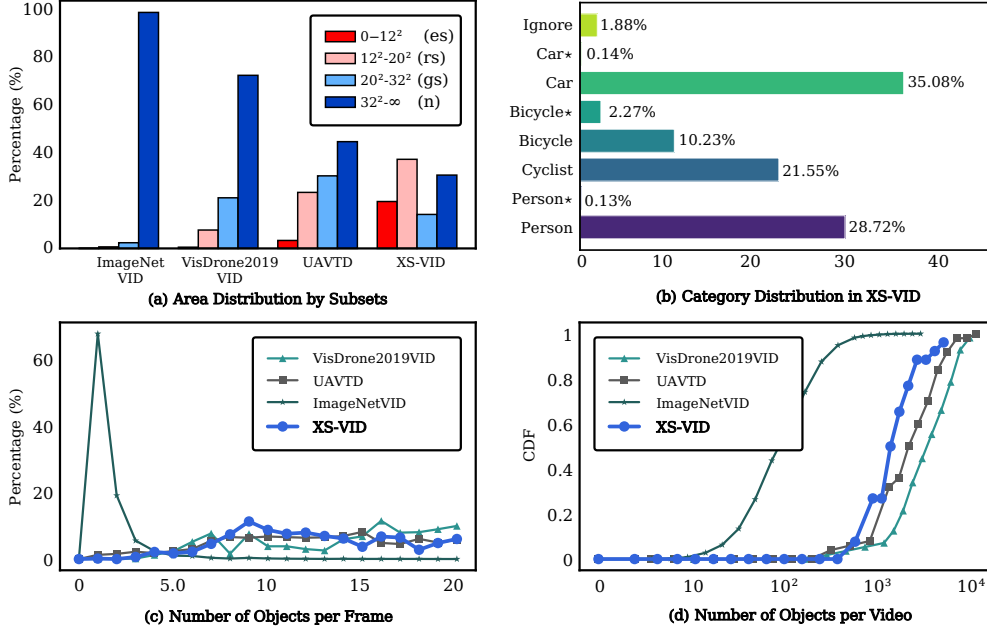


Figure 4: **Quantitative Comparison between XS-VID and various datasets.** The statistical results demonstrate that XS-VID has the highest number of extremely/extremely small objects and the widest area distribution, with a rich and balanced number of objects per frame. * in (b) specifically indicates a high-density aggregation of a particular object.

3 The XS-VID Dataset

We construct a video small object detection dataset named XS-VID through multiple rounds of screening and annotation. This dataset is intended to comprehensively evaluate small video object detection methods. It consists of 38 video segments with a resolution of 1024×1024 , containing 12,230 images and 258,944 object boxes, all with detailed annotation boxes and track annotations. Additionally, it includes movement annotations for specialized designs. The dataset is divided into a training set and a testing set on non-overlapping video scenes, with a ratio of approximately 7:4. See details in appendix A. We also present numerous dataset cases, as detailed in appendix C.

3.1 Data Collection and Annotation

Collection. We used the DJI Air3 drone, flying at an altitude between 70-90m, with a pitch angle of 60-90° and a flight speed of 5-10m/s. Following expert recommendations, data were collected from diverse scenes such as urban streets, main roads, shaded paths, and streams and lakes, encompassing both day and night, as well as autumn and summer. Ultimately, 80 high-definition videos with a resolution of 3840×2160 and a frame rate of 25fps were collected. From these, 38 videos with rich objects and diverse scenes were selected to create the dataset.

Classification. The proposed categories include: person, car, bicycle, cyclist, crowd of people, crowd of cars, crowd of bicycles, and ignore. Annotating objects of extreme sizes is a significant challenge. Especially for person, whose shapes change dramatically in a wide field of view and are easily occluded by leaves, shadows, or others, making them difficult to distinguish in a single frame.

Annotation. After collection and analysis, we found that at a resolution of 3840×2160 , most pedestrians, electric vehicles, and bicycles have pixel sizes around 18×18 , occupying less than 0.01% of the entire image. In this case, it is difficult to distinguish some categories originally differentiated in COCO (e.g., bicycle and motorcycle) with the naked eye, and many objects smaller than people are completely unrecognizable and considered non-objects in practical applications, so they are not included in our classification. For cars, we did not distinguish each type of car individually

as in UAVDT (vehicle detection). Additionally, there is a phenomenon of object aggregation in wide shooting perspectives, especially for people and bicycles, making it difficult to distinguish when they gather. Therefore, we added the Crowd label to assign to clustered objects that are difficult to separate individually. For objects such as mirror reflections, advertisements, and multiple categories clustered in a small area or objects that do not require attention, we uniformly use the ignore label.

We adopted the following annotation steps: 1) Use a general object detector CO-Detr [44] for preliminary annotation. 2) Manually refine and verify the annotations at intervals of 5 to 10 frames [30, 19]. 3) Assign the same ID to the same instance across frames and use image registration interpolation algorithms [16, 17] to fully annotate the entire video, reducing annotation workload. 4) Conduct a fine review and standardization of annotations for the entire video frame by frame, including fine-tuning annotation boxes, deleting and adding unannotated frames, and removing annotations when occlusion is severe to the point of being unrecognizable. 5) For step 4, each video was cross-annotated by 2-3 annotators to merge and obtain the final annotations. Steps 2-4 are very time-consuming. Due to the high image resolution, it is usually necessary to zoom in to 800% of the original size for detailed annotation, making the time cost of searching and annotating objects in each image enormous. Completing the annotation for all frames of a video usually takes 2-4 days.

It is worth noting that we have established unified annotation standards for the following special cases: a) During interval annotation, the first and last frames of the object’s appearance must be specially annotated. b) When objects of the same category appear in clusters causing severe occlusion, they are not annotated individually. c) When objects of multiple categories appear in clusters causing occlusion, blurring, or confusion, they are annotated as ignore; however, if the preliminary annotation model can distinguish each object, they should not be annotated as ignore (strictly limit the use of the ignore label). d) When 50% of a person’s body is occluded, it is not annotated.

Data Post-processing. For the annotated videos, we divide each 3840×2160 resolution video into two 2160×2160 resolution videos along the image width center, with a horizontal overlap of 240 pixels. Finally, we obtain the final videos with a resolution of 1024×1024 through proportional downsampling. This processing aligns with the resolution of most video capture devices and avoids the substantial memory overhead associated with directly inputting overly high-resolution images into the model. It is worth noting that the original resolution videos and their annotations will also be released to support broader research.

Quality Assurance. All videos were annotated by at least two different reviewers. To measure annotation quality, we conducted multiple reviews on a subset of the validation set. Specifically, three reviewers independently annotated the videos frame by frame, and we found high overlap between these independent annotations (IoU exceeding 0.85). Additionally, considering that XS-VID focuses on video object detection, we checked the duration of object appearances and found consistency among different annotators. Overall, the entire annotation process represents approximately 4,000 work-hours of effort.

3.2 Statistical Analysis

We conduct a comprehensive comparison of XS-VID with other significant video detection datasets, including object size distribution, number of object categories, number of instances, total number of images, and total number of videos, as shown in Tab. 1. Additionally, we present an in-depth visual comparison of object size distribution, average number of objects per frame, and average number of objects per video with VisDrone2019VID, UAVDT, and ImageNetVID.

Highest number of extremely small objects and the widest area distribution. Fig. 4(a) shows that the proportion of objects in the size range of $0 \sim 12^2$ and $12^2 \sim 20^2$ in XS-VID is significantly higher than in other datasets. objects in the $0 \sim 12^2$ range account for up to 19.29% (compared to 0.53%, 3.3%, and 0.05% for VisDrone2019VID, UAVDT, and ImageNetVID, respectively), with a median size of only 18×18 . Fig. 4(b) shows the category distribution of XS-VID, containing eight categories (excluding ignore).

Rich and balanced number of objects per frame. As shown in Fig. 4(c), the number of objects per frame in XS-VID is relatively balanced, whereas the number of objects per frame in ImageNetVID is generally 1. Tab. 1 shows the average number of objects per frame, with XS-VID (Avg Obj/Frame:

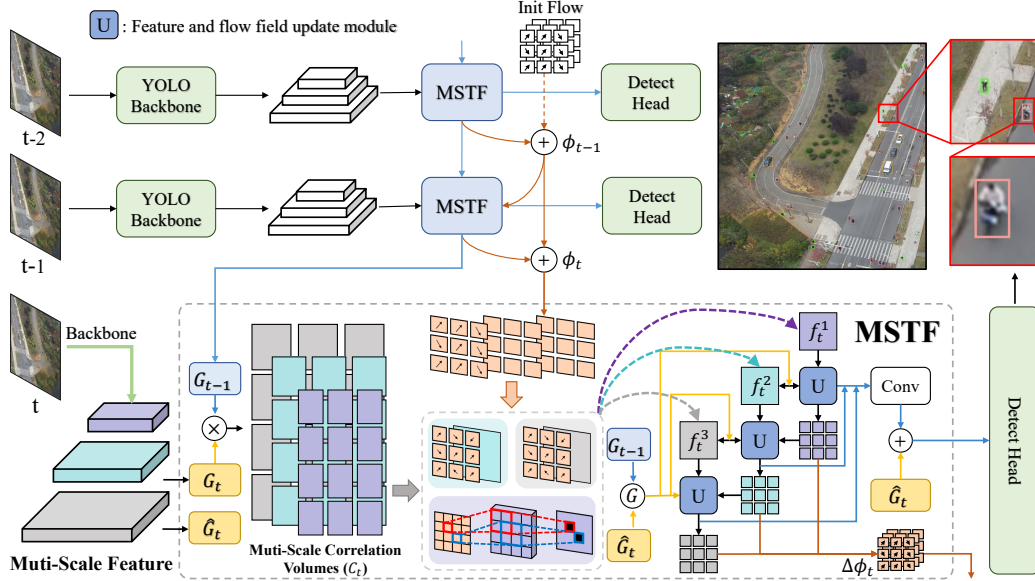


Figure 5: **Overall architecture of our YOLOFT.** Multi-Scale Spatio-Temporal Flow (MSTF) module maintains the optical flow information between consecutive frames and iteratively updates it. Based on this, it extracts multi-scale motion features of the object and integrates them into the static features of the current frame.

22) being the second highest. Additionally, Fig. 4(d) shows the probability distribution of the number of objects per video in XS-VID (CDF, cumulative distribution function, representing the cumulative probability corresponding to different object number ranges). For the same number of objects, the distribution probability of XS-VID is higher compared to VisDrone2019VID and UAVDT, indicating that XS-VID contains a richer number of objects per video.

Table 1: Comparison of Various Datasets for Small Object Video Detection

DataSet	Area Size						Class	Med. Area	Obj/Frame	Instances	Imgs/Vids
	0 ~ 12 ² (es)		12 ² ~ 20 ² (rs)		20 ² ~ 32 ² (gs)						
ImageNet VID [21]	968	0.05%	13k	0.65%	47k	2.36%	30	187 ²	1	2M	1.2M/4417
UAVDT [34]	29k	3.30%	204k	23.03%	265k	29.81%	6	30 ²	22	889K	40k/50
VisDrone2019 [39]	7k	0.53%	115k	7.51%	316k	20.60%	10	45 ²	49	1.5M	30k/58
XS-VID (ours)	49k	19.29%	94k	36.61%	36k	13.97%	8	18 ²	22	260K	12k/38

4 YOLOFT

The overall architecture of the proposed YOLOFT is illustrated in Fig. 5, which consists of a YOLOv8 [12] detector and a temporal fusion Neck, termed the Multi-Scale Spatio-Temporal Flow (MSTF) module, to enhance spatio-temporal feature representation across consecutive frames.

Multi-Scale Correlation Pyramid. The core of the MSTF module is to construct spatio-temporal correlations. To build positional correlation between consecutive frames, we consider that a pixel position (x_i, x_j) in the current feature G_t corresponds to a query space in G_{t-1} within a range $r \in \mathbb{R}^{\max(H/2, W/2)}$. Based on this idea, we constructed the Correlation Pyramid. The design of the Correlation Pyramid is inspired by RAFT [25] for optical flow calculation. However, unlike RAFT, which obtains multi-scale correlation volumes through pooling of single-scale features, MSTF directly constructs multiple correlation volumes between each scale of the feature map $g_t^{(l)}$ and all scales of the previous frame’s feature map $g_{t-1}^{(k)}$. The correlation volume $C_t^{(l,k)}$ for each scale pair (l, k) is defined as:

$$c_t^{(l,k)}(i, j, p, q) = \sum_h g_t^{(l)}(i, j, h) \cdot g_{t-1}^{(k)}(p, q, h), \quad \mathbf{C}_t = \{c_t^{(l,k)}\}_{l,k=0}^m. \quad (1)$$

Table 2: **The main results in XS-VID Test-set and VisDrone2019 VID Test-dev with Single-Frame Object Detectors, Video Object Detectors, Small Object Detectors, YOLO family and YOLOFT.** (The 1st and the 2nd ranking results are highlighted in blue and bold respectively.)

Method		XS-VID					VisDrone2019VID						Param(M)	Time(ms)
		AP	AP _{es}	AP _{rs}	AP _{gs}	AP _m	AP	AP _{es}	AP _{rs}	AP _{gs}	AP _m	AP _l		
VOD	DFE [42]	9.6	0	0.5	4.5	24.4	10.3	0	0.1	3.4	13.6	21.8	120.02	25.5
	FGFA [41]	12.3	0.2	1.1	6.4	30.4	13.6	0	0.9	6.3	17.8	28.5	122.4	181.8
	SELSA [31]	13.6	0	1.7	8.3	33.2	11.8	0	0.5	2.7	14.3	30.2	128.41	110.0
	TROI [10]	12.8	0	1.3	7.6	32.3	12	0	0.1	4.8	16.6	24.7	136.02	285.7
	MEGA [4]	7.8	1.1	2	6.1	25	-	-	-	-	-	-	-	-
	DiffusionVID [20]	10.6	2.7	5.6	9.4	35.4	-	-	-	-	-	-	-	-
	TransVOD [38]	21.8	8.8	13.6	20.5	48.5	9.7	1	3.2	4.9	11.5	23.8	33.78	136.0
GOD	FCOS [26]	24.9	7.7	17.3	22.6	61	12.4	1.3	3.1	4.8	13.8	30.6	32.1	31.8
	ATSS [37]	26.9	8.4	19.2	23.9	68.8	13.7	1.5	4.6	7.2	16.2	29.9	32.1	34.9
	DyHead [7]	23.7	7	15.9	20.5	47.2	9.3	1.4	3.5	5	10.7	20.7	38.906	98.0
	RepPoints [5]	23.7	9.1	18.6	23.9	47.8	13.6	0.7	3.9	5.4	16.3	29	36.8	37.8
	Deformable-DETR [40]	21.3	11.3	13.7	18.7	37.5	9.8	2.5	3.7	5.1	11.9	19.5	40.1	52.3
	Sparse RCNN [24]	21	9	13.9	17.5	28	8.1	1	2.9	4.5	9.5	16	106.0	41.8
	Cascade RPN [27]	27	13.5	19.4	22.1	57.8	12.5	0.9	3.9	6.2	15.1	25.3	41.38	45.3
SOD	CESCE [8]	22.6	10.3	16.2	21.3	48.4	2.5	1.7	3.5	4.4	13	23.8	43.05	31.0
	CFINet [36]	29.5	16.6	21.8	25.1	52.8	12.2	1	3.3	6.3	15.1	25.8	43.9	47.1
YOLO	YOLOX-S [9]	29.1	15	20	25.6	67	7.8	1.6	3.5	5.6	10.4	12.8	8.9	24.0
	YOLOX-L [9]	31	17.4	21.7	25.6	63.8	-	-	-	-	-	-	54.1	37.4
	YOLOV8-S [12]	30	17.8	24.1	27	70.4	13.2	3.9	5	10.1	16.1	22.9	11.17	14.0
	YOLOV8-L [12]	33.6	21.3	27.4	32.7	67.4	16	3.6	5.1	9.9	19.4	27.3	43.69	26.0
	YOLOV9-C [28]	31.6	18.4	24.6	31.2	71	15.5	1.8	5.8	9.8	19.1	33.4	25.54	22.0
	StreamYOLO [33]	33.4	18.7	26.7	33.6	52.8	17.6	1.6	5.1	10.4	22.3	33.7	698.08	48.0
Ours	YOLOFT-S	33.2	21.5	27.9	33.2	67.3	14.8	4.4	6.1	10.8	16.4	26.2	12.84	16.0
	YOLOFT-L	36.4	24.7	28.9	33.4	78.2	15.8	4.9	6.5	11.8	19.4	25.8	45.16	36.0

Here, i and j are the pixel positions in the current frame’s scale l , and p and q are the pixel positions in the previous frame’s scale k . We construct a multi-scale pyramid as $[c^{(0,0)}, c^{(0,2)}, \dots, c^{(0,m)}], \dots, [c^{(m,0)}, c^{(m,2)}, \dots, c^{(m,m)}]$. For the same level of the pyramid, the last two dimensions are reduced by a stride of 2, so the dimensions of $c^{(l,k)}$ are: $H/2^l \times W/2^l \times H/2^k \times W/2^k$. This ensures that each pixel at each scale can obtain different scale similarities from the previous frame, which is crucial for detection. It captures both large and small movements while retaining high-resolution information, fully utilizing the motion and static features of objects. The final structure of the multi-scale correlation pyramid is represented as C_t .

Multi-Scale Correlation Lookup. We use the lookup operator L_C from RAFT [25] to obtain motion information of the object in the current feature map. This operator uses optical flow $\phi_{t \rightarrow t-1}$ to perform lookups across all levels of the correlation pyramid, providing similarity metrics between local regions of corresponding pixels across frames. For the feature at level l , the corresponding correlation pyramid is $\{c_t^{(l,k)}\}_{k=1}^m$. In our design, the sampling radius r is consistent across all levels, ensuring that lower levels encompass a larger context. Finally, we concatenate values from each level into a single feature map f .

Feature Update. With the correlated feature map f obtained between consecutive frames, containing motion information, we update the current static features and optical flow estimates. The update operation(details shown in Fig. 5) is defined as follows:

$$\begin{aligned} \hat{G}_t^{(l)}, \Delta\phi_t^{(l)} &= \text{Update} \left(G_t^{(l)}, G_{t-1}^{(l)}, c_t^{(l)}, f_t^{(l)}, \text{interp}(f_t^{(l-1)}) \right) \\ \phi_t^{(l)} &\leftarrow \phi_t^{(l)} + \Delta\phi_t^{(l)}. \end{aligned} \quad (2)$$

Here, $\text{interp}(\cdot)$ represents the flow field estimate at the current scale l obtained by upsampling and interpolating from the lower scale $l-1$. The GRU unit is responsible for fusing the current flow estimate, multi-scale correlation information, and information interpolated from the lower scale.

5 Experiments

5.1 Comparison with State-of-the-art Detection Methods

Tab. 2 shows the evaluation results of these methods on XS-VID and VisDrone2019VID. Notably, we did not provide the AP_l for the large subset in XS-VID because large objects account for only 1%

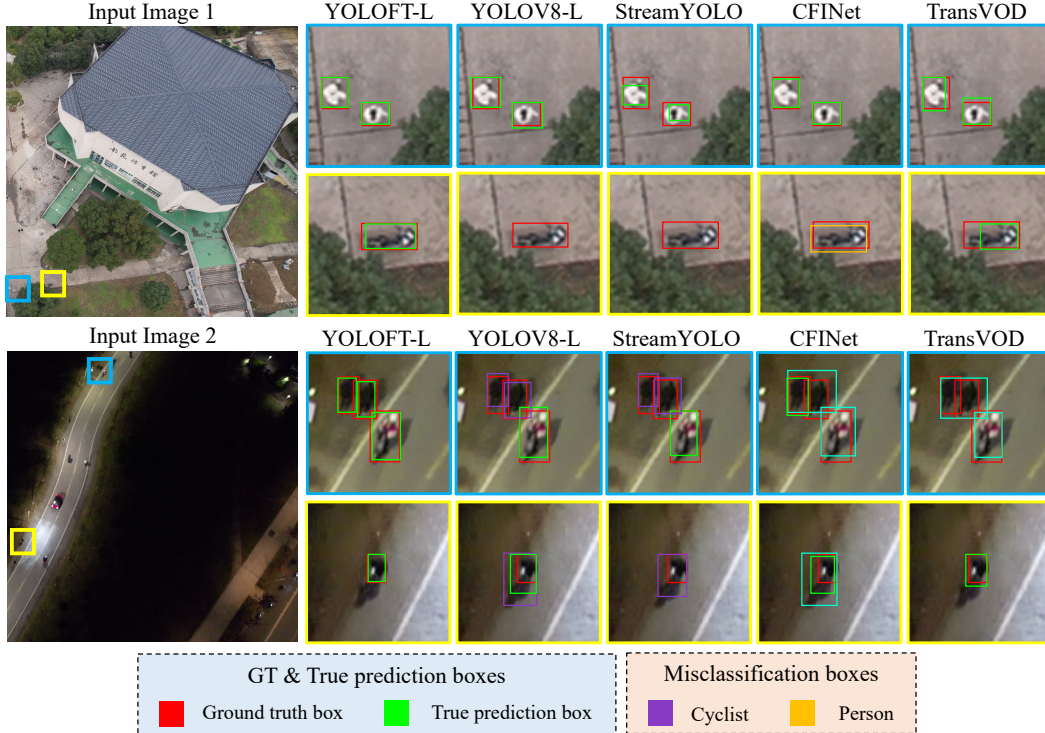


Figure 6: **Visual comparison of our YOLOFT and other baseline detectors.** Our YOLOFT achieves the most accurate predictions matching the GT boxes in both day and night scenes, significantly outperforming other methods. See paragraph 5.1 for detailed description.

of XS-VID and do not reflect the detection results well. Additionally, we exclude TransVisDrone from the accuracy ranking as its inference time exceeds 2 seconds, making it unsuitable for real-time scenarios addressing small object issues.

Extreme sizes lead to poor detection performance for many methods. Especially for VOD methods, the detection results for small objects (*es*, *is*, *gs*) are very low, with some methods scoring even 0. This indicates that current VOD methods are unsuitable for small object detection. The main reason is that existing VOD methods are primarily designed and evaluated on ImageNetVID, where the objects are too large, occupying almost the entire frame. This leads these methods to focus on deeper feature designs, resulting in the near-total loss of small object information. However, the modeling and feature enhancement for motion objects in VOD methods are valuable.

Complex designs do not significantly enhance small object detection performance. Cascade RPN is a general two-stage detector that already shows good detection performance compared to many other methods. Similarly, the two-stage network CFINet, specifically designed for small objects, does not significantly improve performance and still falls short compared to the YOLO series. Likewise, CESCE, which focuses on small object detection, performs even worse.

Anchor-free single-stage detectors perform the best. Whether on XS-VID or the publicly available VisDrone2019VID dataset, single-stage detectors perform the best overall, especially the YOLO series (Fig. 3). We found that single-frame detectors optimized through structural and gradient improvements can retain small object information well, achieving good detection accuracy even with only texture features.

Incorporating optical flow-based motion features into YOLO achieves the best detection performance. Inspired by optical flow methods and based on comprehensive evaluation results, YOLOFT enhances multi-scale feature representation with motion information between consecutive frames. Through optimizations in time consumption and multi-scale information fusion, YOLOFT achieves

Table 3: Different gradient division ratios (motion features via optical flow)

Static:Motion	AP	AP _{es}	AP _{rs}	AP _{gs}
1:3	33.5	21.9	26.3	32.7
3:1	33.2	21.5	27.9	33.5
1:1	32.6	21.3	26.2	33.6
1:0	32.3	20.5	25.4	33.5

Table 5: Using multi-scale flow to guide feature fusion: 8, 16, and 32 represent the down-sampling ratios.

Flow Level	AP	AP _{es}	AP _{rs}	Time(ms)
16	32.8	20.6	25.6	15.6
8+16+32	32.6	21.3	26.2	18.6
8	32.5	19.8	25.8	16.2
32	32.3	20.7	25.4	15.5

Table 4: Different data enhancement(D: Degree,S: Scale,P: perspective)

[D, S, P]	AP	AP _{es}	AP _{rs}	AP _{gs}
[2,0,0,2,1e-4]	32.6	21.3	26.2	33.6
No argument	32.3	20	26.4	33.2
[0,0,0,5,1e-3]	32.1	20.8	25.3	33.1
[0,0,0,0,1e-3]	31.8	20.6	26.4	32.6

Table 6: Timing of motion feature fusion: indicates that only static features are trained epoch from 0 – n.

Epoch n	AP	AP _{es}	AP std	AP _{es} std
4	32.6	21.3	0.21	0.27
8	32.6	21.2	0.17	0.35
0	32.3	20.6	0.4	0.42
6	32.2	19.9	0.19	0.37

an AP of 36.2 (+7.7%) on XS-VID. AP_{es} is 25.4 (+19.2%), and the best performance in AP_{es}, AP_{rs}, and AP_{gs} on VisDrone2019VID.

Visual comparison of Various Methods on our XS-VID. As shown in Fig. 6, we present the visualization results of YOLOFT and various state-of-the-art methods, including YOLOv8, StreamYOLO, CFINet, and TransVOD. In nighttime scenarios, we observe significant misclassification issues with previous advanced detectors. Moreover, when texture features are mixed with complex backgrounds, methods like YOLOv8 and StreamYOLO exhibit missed detections. In contrast, YOLOFT alleviates classification problems in confusing scenes and achieves better alignment between predicted and ground truth bounding boxes. This further validates the effectiveness of our approach.

5.2 Design Considerations for Small Video Object Detection

In this section, we conduct ablation experiments on our YOLOFT using the YOLOFT-S model (see Appendix B for YOLOFT-L’s results) to investigate important factors affecting the detection of small objects with severe texture degradation.

Quality Motion Gradient Information is Essential for Small Object Feature Extraction. Our study found that complex multi-frame integration designs in video detectors often lead to elongated gradient flows and weak feature responses for small objects, hampering effective weight updates and causing interference between motion and static features. The YOLO series methods achieve optimal performance by maintaining excellent gradient backpropagation without redundant components. We retained the original gradient architecture, segmented static features, and transformed only a portion before merging with static feature residuals. Tab. 3 shows the impact of different ratios of motion and static feature segmentation on model accuracy. Results indicate that a 1:0 ratio performs the worst, while ratios of 1:3 or 3:1 yield better performance than 1:1. A predominance of motion information (static:motion = 1:3) results in the highest detection accuracy(AP is 33.5,AP_{es} is 21.9).

High-quality static features enhance detection robustness. Many video detectors emphasize motion feature extraction over static feature extraction, making it difficult to learn high-quality static features. In XS-VID, we found that good static features significantly increase detector robustness and improve overall accuracy. As shown in Tab. 6, repeating experiments 10 times revealed that starting with feature fusion results in high standard deviations for key AP and AP_{eg} (0.4 and 0.42, respectively). Training the static backbone first and then fusing motion features reduced standard deviations by more than half and slightly improved accuracy by 0.3 points.

Local optical flow information is useful for small objects. Using optical flow to warp information from different times can aid detection, but in XS-VID, extreme object sizes and camera movement make it difficult to learn optical flow warping for entire frames. Introducing local optical flow

information reduces computation time and avoids noise. As shown in Tab. 5, using the highest resolution scale (level 8) achieved the best accuracy (+0.2), and using all scales with fusion improved AP_{eg} the most (+0.7).

Appropriate video-level data augmentation improves small object detection. We explored the impact of spatial transformations during XS-VID training. As shown in Tab. 4, transformations such as Degree, Scale, and perspective, similar to drone shooting angles, were examined. Introducing small transformation variations improved AP_{eg} by 7% and slightly improved overall AP. However, excessive transformations caused severe object deformation, reducing model performance.

6 Conclusion

In this work, we first analyzed that existing SVOD datasets are scarce and suffer from issues such as insufficiently small objects, limited object categories, and lack of scene diversity, leading to unitary application scenarios for corresponding methods. Due to these issues, the previous state-of-the-art methods tend to struggle. To address this gap, we proposed the XS-VID dataset, which comprises aerial data from various periods and scenes, and annotates eight major object categories. XS-VID extensively collects three types of objects with smaller pixel areas: extremely small (es , $0 \sim 12^2$), relatively small (rs , $12^2 \sim 20^2$), and generally small (gs , $20^2 \sim 32^2$). In general, XS-VID offers the most comprehensive coverage of miniature object sizes ($0 \sim 32^2$), the largest number and proportion of es (extremely small, $\leq 12^2$) objects, and the widest range of scene types, effectively filling the data gap. Next, we analyzed the challenges in SVOD and conducted comprehensive experiments to reveal the performance of various advanced detection methods on the proposed XS-VID dataset. Also, we observed that these methods often perform poorly due to a lack of consideration for extremely small objects in existing datasets. Finally, we proposed YOLOFT, which significantly improves the accuracy and stability of SVOD by enhancing local feature associations and integrating temporal motion features of objects. We conducted extensive experiments on XS-VID and VisDrone2019VID, and the results consistently demonstrate that YOLOFT achieves SOTA performance. We have released our entire dataset and the benchmarks, hoping our dataset leads to further advancements in SVOD.

References

- [1] Yancheng Bai, Yongqiang Zhang, Mingli Ding, and Bernard Ghanem. Finding tiny faces in the wild with generative adversarial network. In 2018 IEEE/CVF Conference on Computer Vision and Pattern Recognition, pages 21–30, 2018.
- [2] Changrui Chen, Yu Zhang, Qingxuan Lv, Shuo Wei, Xiaorui Wang, Xin Sun, and Junyu Dong. Rrnet: A hybrid detector for object detection in drone-captured images. In 2019 IEEE/CVF International Conference on Computer Vision Workshop (ICCVW), pages 100–108, 2019.
- [3] Kai Chen, Jiaqi Wang, Jiangmiao Pang, Yuhang Cao, Yu Xiong, Xiaoxiao Li, Shuyang Sun, Wansen Feng, Ziwei Liu, Jiarui Xu, Zheng Zhang, Dazhi Cheng, Chenchen Zhu, Tianheng Cheng, Qijie Zhao, Buyu Li, Xin Lu, Rui Zhu, Yue Wu, Jifeng Dai, Jingdong Wang, Jianping Shi, Wanli Ouyang, Chen Change Loy, and Dahua Lin. MMDetection: Open mmlab detection toolbox and benchmark. arXiv preprint arXiv:1906.07155, 2019.
- [4] Yihong Chen, Yue Cao, Han Hu, and Liwei Wang. Memory enhanced global-local aggregation for video object detection. In Proceedings of the IEEE/CVF Conference on Computer Vision and Pattern Recognition (CVPR), June 2020.
- [5] Yihong Chen, Zheng Zhang, Yue Cao, Liwei Wang, Stephen Lin, and Han Hu. Reppoints v2: Verification meets regression for object detection. Advances in Neural Information Processing Systems, 33:5621–5631, 2020.
- [6] MMTracking Contributors. MMTracking: OpenMMLab video perception toolbox and benchmark. <https://github.com/open-mmlab/mtracking>, 2020.
- [7] Xiyang Dai, Yinpeng Chen, Bin Xiao, Dongdong Chen, Mengchen Liu, Lu Yuan, and Lei Zhang. Dynamic head: Unifying object detection heads with attentions, 2021.
- [8] Bowei Du, Yecheng Huang, Jiabin Chen, and Di Huang. Adaptive sparse convolutional networks with global context enhancement for faster object detection on drone images. In Proceedings of the IEEE/CVF Conference on Computer Vision and Pattern Recognition (CVPR), pages 13435–13444, June 2023.
- [9] Zheng Ge, Songtao Liu, Feng Wang, Zeming Li, and Jian Sun. Yolox: Exceeding yolo series in 2021, 2021.
- [10] Tao Gong, Kai Chen, Xinjiang Wang, Qi Chu, Feng Zhu, Dahua Lin, Nenghai Yu, and Huamin Feng. Temporal roi align for video object recognition. Proceedings of the AAAI Conference on Artificial Intelligence, 35(2):1442–1450, May 2021.
- [11] Yecheng Huang, Jiabin Chen, and Di Huang. Ufmp-det: Toward accurate and efficient object detection on drone imagery. In AAAI Conference on Artificial Intelligence, 2022.
- [12] Glenn Jocher, Ayush Chaurasia, and Jing Qiu. Ultralytics YOLO, January 2023.
- [13] Jung Uk Kim, Sungjune Park, and Yong Man Ro. Robust small-scale pedestrian detection with cued recall via memory learning. In 2021 IEEE/CVF International Conference on Computer Vision (ICCV), pages 3030–3039, 2021.
- [14] Mate Kisanal, Zbigniew Wojna, Jakub Murawski, Jacek Naruniec, and Kyunghyun Cho. Augmentation for small object detection, 2019.
- [15] Jing Li, Dong Hye Ye, Mathias Kolsch, Juan P. Wachs, and Charles A. Bouman. Fast and robust uav to uav detection and tracking from video. IEEE Transactions on Emerging Topics in Computing, 10(3):1519–1531, 2022.
- [16] David G Lowe. Distinctive image features from scale-invariant keypoints. International journal of computer vision, 60:91–110, 2004.
- [17] Marius Muja and David G Lowe. Fast approximate nearest neighbors with automatic algorithm configuration. VISAPP (1), 2(331-340):2, 2009.
- [18] Junhyug Noh, Wonho Bae, Wonhee Lee, Jinhwan Seo, and Gunhee Kim. Better to follow, follow to be better: Towards precise supervision of feature super-resolution for small object detection. In 2019 IEEE/CVF International Conference on Computer Vision (ICCV), pages 9724–9733, 2019.
- [19] open mmlab. playground. <https://github.com/open-mmlab/playground>, 2023.
- [20] Si-Dong Roh and Ki-Seok Chung. Diffusionvid: Denoising object boxes with spatio-temporal conditioning for video object detection. IEEE Access, 2023.
- [21] Olga Russakovsky, Jia Deng, Hao Su, Jonathan Krause, Sanjeev Satheesh, Sean Ma, Zhiheng Huang, Andrej Karpathy, Aditya Khosla, Michael Bernstein, et al. Imagenet large scale visual recognition challenge. International journal of computer vision, 115:211–252, 2015.
- [22] Tushar Sangam, Ishan Rajendrakumar Dave, Waqas Sultani, and Mubarak Shah. Transvisdrone: Spatio-temporal transformer for vision-based drone-to-drone detection in aerial videos, 2023.

- [23] Yuheng Shi, Naiyan Wang, and Xiaojie Guo. Yolov: Making still image object detectors great at video object detection, 2023.
- [24] Peize Sun, Rufeng Zhang, Yi Jiang, Tao Kong, Chenfeng Xu, Wei Zhan, Masayoshi Tomizuka, Lei Li, Zehuan Yuan, Changhu Wang, et al. Sparse r-cnn: End-to-end object detection with learnable proposals. In Proceedings of the IEEE/CVF conference on computer vision and pattern recognition, pages 14454–14463, 2021.
- [25] Zachary Teed and Jia Deng. Raft: Recurrent all-pairs field transforms for optical flow, 2020.
- [26] Zhi Tian, Chunhua Shen, Hao Chen, and Tong He. Fcos: Fully convolutional one-stage object detection, 2019.
- [27] Thang Vu, Hyunjun Jang, Trung X. Pham, and Chang D. Yoo. Cascade rpn: Delving into high-quality region proposal network with adaptive convolution, 2019.
- [28] CY Wang, IH Yeh, and HYM Liao. Yolov9: Learning what you want to learn using programmable gradient information. arxiv 2024. [arXiv preprint arXiv:2402.13616](https://arxiv.org/abs/2402.13616).
- [29] Huan Wang, Luping Zhou, and Lei Wang. Miss detection vs. false alarm: Adversarial learning for small object segmentation in infrared images. In 2019 IEEE/CVF International Conference on Computer Vision (ICCV), pages 8508–8517, 2019.
- [30] Wei Wang. Advanced auto labeling solution with added features. <https://github.com/CVHub520/X-AnyLabeling>, 2023.
- [31] Haiping Wu, Yuntao Chen, Naiyan Wang, and Zhaoxiang Zhang. Sequence level semantics aggregation for video object detection. ICCV 2019, 2019.
- [32] Jialian Wu, Chunluan Zhou, Qian Zhang, Ming Yang, and Junsong Yuan. Self-mimic learning for small-scale pedestrian detection. In Proceedings of the 28th ACM International Conference on Multimedia, pages 2012–2020, 2020.
- [33] Jinrong Yang, Songtao Liu, Zeming Li, Xiaoping Li, and Jian Sun. Real-time object detection for streaming perception, 2022.
- [34] Hongyang Yu, Guorong Li, Weigang Zhang, Qingming Huang, Dawei Du, Qi Tian, and Nicu Sebe. The unmanned aerial vehicle benchmark: Object detection, tracking and baseline. International Journal of Computer Vision, 128:1141–1159, 2020.
- [35] Xuehui Yu, Yuqi Gong, Nan Jiang, Qixiang Ye, and Zhenjun Han. Scale match for tiny person detection. In Proceedings of the IEEE/CVF winter conference on applications of computer vision, pages 1257–1265, 2020.
- [36] Xiang Yuan, Gong Cheng, Kebin Yan, Qinghua Zeng, and Junwei Han. Small object detection via coarse-to-fine proposal generation and imitation learning. In Proceedings of the IEEE/CVF International Conference on Computer Vision (ICCV), pages 6317–6327, October 2023.
- [37] Shifeng Zhang, Cheng Chi, Yongqiang Yao, Zhen Lei, and Stan Z Li. Bridging the gap between anchor-based and anchor-free detection via adaptive training sample selection. In Proceedings of the IEEE/CVF conference on computer vision and pattern recognition, pages 9759–9768, 2020.
- [38] Qianyu Zhou, Xiangtai Li, Lu He, Yibo Yang, Guangliang Cheng, Yunhai Tong, Lizhuang Ma, and Dacheng Tao. Transvod: End-to-end video object detection with spatial-temporal transformers. IEEE Transactions on Pattern Analysis and Machine Intelligence, 45(6):7853–7869, 2023.
- [39] Pengfei Zhu, Longyin Wen, Dawei Du, Xiao Bian, Heng Fan, Qinghua Hu, and Haibin Ling. Detection and tracking meet drones challenge. IEEE Transactions on Pattern Analysis and Machine Intelligence, 44(11):7380–7399, 2021.
- [40] Xizhou Zhu, Weijie Su, Lewei Lu, Bin Li, Xiaogang Wang, and Jifeng Dai. Deformable detr: Deformable transformers for end-to-end object detection. [arXiv preprint arXiv:2010.04159](https://arxiv.org/abs/2010.04159), 2020.
- [41] Xizhou Zhu, Yujie Wang, Jifeng Dai, Lu Yuan, and Yichen Wei. Flow-guided feature aggregation for video object detection. In Proceedings of the IEEE International Conference on Computer Vision (ICCV), Oct 2017.
- [42] Xizhou Zhu, Yuwen Xiong, Jifeng Dai, Lu Yuan, and Yichen Wei. Deep feature flow for video recognition. In Proceedings of the IEEE Conference on Computer Vision and Pattern Recognition (CVPR), July 2017.
- [43] Yichen Zhu, Qiqi Zhou, Ning Liu, Zhiyuan Xu, Zhicai Ou, Xiaofeng Mou, and Jian Tang. Scalekd: Distilling scale-aware knowledge in small object detector. In Proceedings of the IEEE/CVF Conference on Computer Vision and Pattern Recognition, pages 19723–19733, 2023.
- [44] Zhuofan Zong, Guanglu Song, and Yu Liu. Detsr with collaborative hybrid assignments training, 2022.

A XS-VID Data Details

A.1 Data Splits

We selected 12 fully annotated videos as the test set, ensuring that their shooting locations do not appear in the remaining 26 videos. Additionally, these 12 videos include scenes not present in the training set. This maximizes the evaluation of the model’s generalization and robustness.

Table 7: Data split for XS-VID.

Split	# of Videos	# of Images	# of Instances
Train	26	7426	151K
Test	12	4212	108K
Total	38	11638	259K

A.2 XS-VID Object Distribution

In the main text, we compared XS-VID with existing datasets. This section focuses on the object distribution within XS-VID itself. We present the aspect ratio distribution of the objects, highlighting the wide variety of aspect ratios in XS-VID, which poses significant challenges.

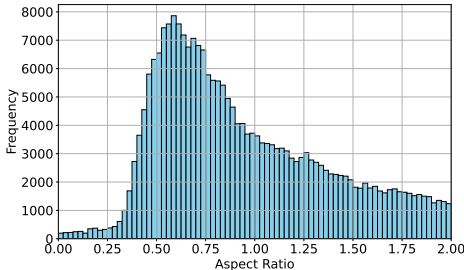


Figure 7: Object aspect ratio distribution of XS-VID.

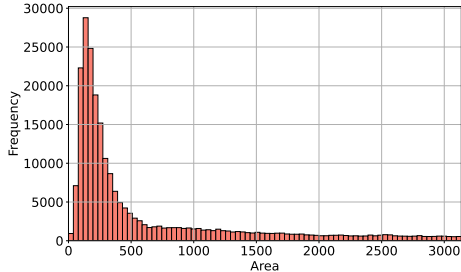


Figure 8: Object area distribution of XS-VID.

A.3 XS-VID Movement Attribute

Besides standard annotations, we provide an attribute indicating whether an object is moving. For objects that frequently start and stop, practical considerations guide the labeling. For instance, a vehicle that is about to start moving will be labeled as moving even at very slow speeds, and similarly, a vehicle about to stop will be labeled as stationary at very slow speeds. Similar rules apply to other objects. Due to inherent ambiguity, we average annotations in areas with discrepancies during cross-annotation. For example, if one annotation marks an object as moving from frames 0 to 10 and another from frames 4 to 16, we average this to label the object as moving from frames 2 to 13. Fig. 9 shows the distribution of moving objects within each category.

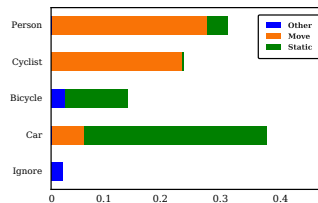


Figure 9: Distribution of moving objects within each category in XS-VID. Here, * indicates aggregated annotations for the current category, and B.P. refers to a person riding a bicycle.

B Ablation Studies on YOLOFT

We conducted comprehensive ablation studies on our baseline method YOLOFT. Sec. 5.2 includes some experimental results, and this section presents additional ablation results, including ablations with different model sizes.

Removing the Temporal Fusion Module. We removed the core improvement module of YOLOFT, degrading it to a YOLOV8 model for ablation experiments. The results are shown in Tab. 8. Our method comprehensively surpasses YOLOV8 in accuracy while still meeting real-time computation requirements (at least 25fps, 40ms).

Table 8: Ablation experiments with YOLOft and its baseline

Method	AP	AP _{es}	AP _{rs}	AP _{gs}	AP _m	Time(ms)
Baseline-S	30.0	17.8	24.1	27.0	70.4	14
YOLOFT-S	33.2	21.5	27.9	33.2	67.3	16
Baseline-L	33.6	21.3	27.4	32.7	67.4	26
YOLOFT-L	36.2	25.4	28.1	33.3	72.3	36

Impact of Local Sampling Radius of the Core Operator. The core of YOLOFT is sampling local features from historical frames to model object motion. The local sampling radius from historical frames represents an important receptive field in the time dimension. The experimental results on YOLOFT-S are shown in Tab. 9(a), and those on YOLOFT-L are shown in Tab. 9(b).

Table 9: Impact of localized sampling radius in YOLOFT-S and YOLOFT-L

[r ₀ ,r ₁ ,r ₂]	AP	AP _{es}	AP _{rs}	AP _{gs}	Time(ms)	[r ₀ ,r ₁ ,r ₂]	AP	AP _{es}	AP _{rs}	AP _{gs}	Time(ms)
[5,4,3]	32.8	19.8	26.2	37.1	22.6	[3,2,4]	36.3	24.8	29.6	35.4	37
[3,4,5]	32.8	19.8	26.1	35.6	18.2	[3,3,3]	36.2	25.4	28.6	33.4	36
[4,3,5]	32.7	20.2	24.8	32.8	21.6	[2,2,3]	36	24.9	29.3	34.1	33.7
[4,4,4]	32.6	21.3	26.2	33.6	18.8	[2,3,4]	35.8	24.9	29	34.6	35.2
[4,5,3]	32.2	19.1	25.1	35.7	22	[4,3,2]	35.6	24.5	29.4	34.6	40.2
[3,3,4]	32.2	19.0	25.3	33.9	18.0	[4,4,3]	35.5	24.6	29.1	33.7	42.2
[5,5,4]	31.8	18.9	25.4	32.5	24.3	[3,4,2]	35.5	24.4	28.4	35	38.7

(a) YOLOFT-S

(b) YOLOFT-L

Table 10: Number of single optical flow optimizations in YOLOFT-S and YOLOFT-L

flow iters	AP	AP _{es}	AP _{rs}	AP _{gs}	Time(ms)	flow iters	AP	AP _{es}	AP _{rs}	AP _{gs}	Time(ms)
3	33.5	20.7	26.3	39.7	35.9	2	36.5	23.9	28.8	36.8	48.1
2	32.7	20.5	26.3	35.6	28.4	1	36.2	25.4	28.6	33.4	36
1	32.6	21.3	26.2	33.6	18.6	4	35.7	23.9	29.6	36.6	70.3
4	32.2	19.4	25.3	35.1	43.9	3	35.6	24	28.9	33.7	60.9

(a) YOLOFT-S

(b) YOLOFT-L

Impact of Iteration Times for Optical Flow Estimation. YOLOFT assumes smooth changes in optical flow throughout the video, updating it based on the similarity between consecutive frames. We explored how different update iterations affect model accuracy. The experimental results on YOLOFT-S are shown in Tab. 10(a), and those on YOLOFT-L are shown in Tab. 10(b).

Impact of Multi-Scale Optical Flow Information. Sec. 5.2 presents the detection results of small objects guided by multi-scale optical flow information in YOLOFT-S. Supplementary results on YOLOFT-L are shown in Tab. 11. The results align with those on YOLOFT-S, showing that higher resolution information positively impacts smaller objects. Unlike the S model, the L model achieves even higher performance after integrating information from three scales.

Table 11: Using multi-scale flow to guide feature fusion: 8, 16, and 32 represent the down-sampling ratios.

Flow Level	AP	AP _{es}	AP _{rs}	AP _{gs}	Time(ms)
8+16+32	36.2	25.4	28.6	33.4	36
32	35.9	24.1	29.4	34.9	33.6
16	35.8	24.3	29.7	34.4	35.2
8	35.7	25.6	28.7	34.4	34.3

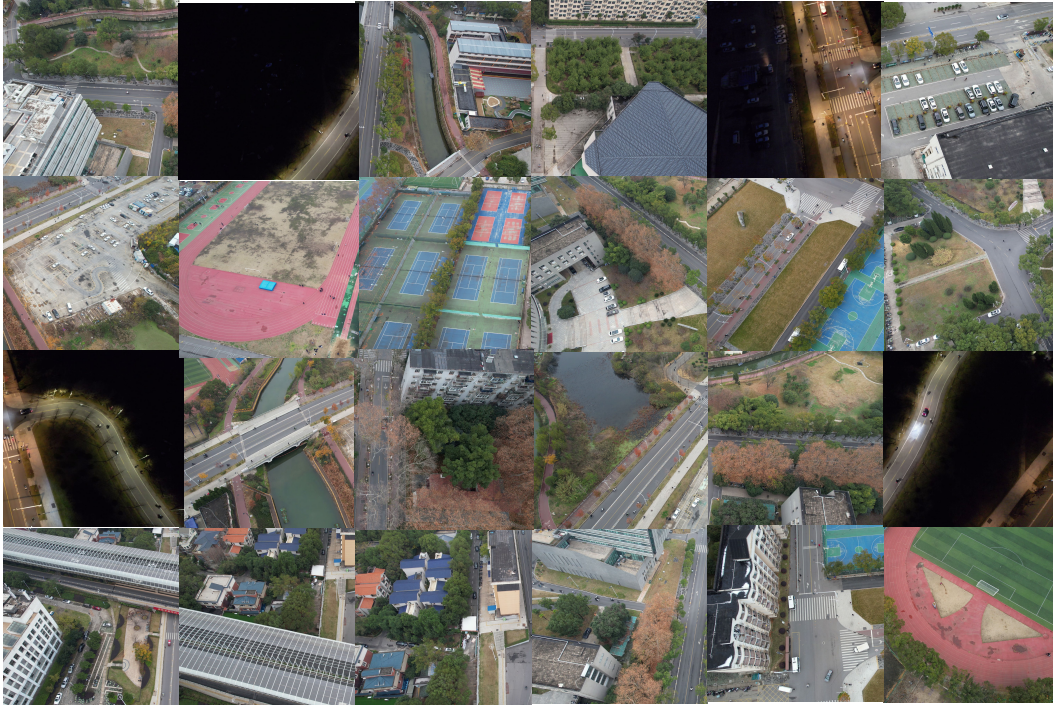


Figure 10: Visualization cases of XS-VID Dataset.

C Visualization cases of XS-VID Dataset

As shown in Fig. 10, we present some cases of XS-VID for reference, demonstrating various scenes such as roads, forests, buildings, bridges, and day and night environments.

D Experimental Setup

For all GOD methods and YOLOX, we used mmdetection [3] for testing. For some VOD methods ([42, 41, 31, 10]), we used mmtracking [6]. Some YOLO methods were tested using Ultralytics [12]. Other methods were tested using the official code provided by the original papers. During testing, we only modified the dataset and set the training and testing image size to 1024x1024, faithfully following the configurations in the original papers. Our machine is equipped with an NVIDIA RTX 3090.

E Limitations

The bounding box annotations were performed by human annotators. Despite multiple rounds of review and cross-annotation to ensure accuracy and consistency, there may still be human errors or biases. Additionally, due to the nature of drone flights, there may be some inaccuracies in determining the first and last frames for objects entering and exiting the frame, leading to poor annotations for

frequently moving objects. Although XS-VID has a rich variety of objects, the absolute number of objects and frames is only moderate, and further development requires expanding the dataset.

Furthermore, our baseline method YOLOFT also has some limitations. We have discovered that YOLOFT's local optical flow cannot effectively capture the motion characteristics of larger objects, leading to misidentification of larger objects.

F Potential Negative Societal Impacts

Our videos are collected from drone flights, which may have several potential negative impacts. We summarize a few scenarios:

There may be privacy risks and there may be data imbalances, such as geographic and category distribution. This risk can be mitigated by future collaborations in underrepresented areas.

- **Privacy and Ethical Impacts:** For example, individuals and vehicles recorded in the videos. We have edited and obscured footage that may reveal privacy and have developed a user agreement to ensure legal and compliant use of the data.
- **Security Risks:** Small object detection is commonly used in surveillance and security. This dataset could be used to train systems for criminal activities. To mitigate this risk, we have rigorously screened and reviewed the data to remove any that could be used for malicious purposes before releasing it.
- **Data Bias and Fairness Issues:** Such as geographic and category distribution. This risk can be mitigated with future work that grows the collaboration in underrepresented areas.